Chitosan-derived biochars obtained at low pyrolysis temperatures for potential application in electrochemical energy storage devices

Roberto Nisticò[a,*,1], Federico Guerretta[b], Paola Benzi[b], Giuliana Magnacca[b,c]

[a]Polytechnic of Torino, Department of Applied Science and Technology DISAT, C.so Duca degli Abruzzi 24, 10129 Torino, Italy.

[b]University of Torino, Department of Chemistry, Via P. Giuria 7, 10125 Torino, Italy.

[c]NIS Centre, Via P. Giuria 7, 10125 Torino, Italy.

*Corresponding author E-mail address: roberto.nistico0404@gmail.com (R. Nisticò).

[1]Current address: Independent Researcher, Via Borgomasino 39, 10149 Torino, Italy.

Abstract

N-rich biochars were obtained via pyrolysis treatment of chitosan (a low-cost biopolymer from natural biomasses) at mild conditions (in the 284 °C–540 °C range), thus offering an energy efficient and low carbon footprint synthesis. These low surface area N-doped biochars were morphologically and physicochemically characterized, and tested as hosting material in lithium-sulfur (Li-S) batteries. Sulfur/biochars cathodes thus obtained showed good capacity retention and improved Coulombic efficiency compared to a standard N-rich high surface area carbon and multiwalled carbon nanotubes (MWCNT) reference substrates. Such enhanced electrochemical properties are attributable to the better retention of Li polysulfides by means of the residual functionalities still present in the biochars, thus making the valorization of chitosan potentially appealing even in the industrial sector related to the development of energy storage devices.

Keywords: Biochars; Chitosan; Lithium-sulfur batteries.

1. Introduction

The growing demand of sustainable feedstock to produce advanced materials, as alternative technological solutions to more traditional fossil-derived chemicals, is rapidly increasing in the last decades, becoming a mandatory target for the next future development [1–5]. In this context, the valorization of biomasses and natural products to produce carbon-based materials attracted the attention of the scientific community due to the positive integration of these carbonaceous nanostructures into several challenging fields, very attractive from both the technological and industrial viewpoint, such as: catalysis [6], sensing [7], environmental remediation and separation science [8–11], CO_2 sequestration [12], agriculture [13], energetic development (e.g., batteries and other energy storage devices) [14–16], engineering (e.g., reinforced/functional composites) [17–20], and many others.

Moreover, the isolation of bio-based products from aquatic-derived biomasses is a very attractive solution, considering that aquatic environments cover more than 70% of the planet surface [21,22]. According to the literature, chitosan (i.e., a natural polysaccharide derived from the shellfish industry) is widely recognized being a very promising biopolymer due to its advanced properties which allow its use in biomedicine/surgery [23–25], cosmetics [26], wastewater treatments [27–29], food packaging [30], and agriculture industry [31]. Being a carbohydrate, chitosan can be easily converted into chars by simply performing carbonization processes under controlled atmosphere

(i.e., pyrolysis) [32]. According to the International Biochar Initiative (IBI), the term "biochar" refers to thermal decomposition processes performed at temperatures below 700 °C [33]. The literature concerning the production of biochars from chitosan is quite large, but in the majority of the cases pyrolysis conditions were set at temperatures higher than 700 °C [34–37], whereas milder conditions were preferentially adopted in other processes (e.g., hydrothermal carbonization) [38]. However, according to literature [9,16,39–41], it is possible to successfully convert different biomasses into functional N-doped biochars via pyrolysis treatments performed at low temperatures (i.e., below 540 °C), and only in few cases performances of chitosan-derived biochars at mild conditions were evaluated [32].

Among the possible industrial applications of biochars, their exploitation in next generation lithium-sulfur (Li-S) batteries surely is widely recognized as striking [42]. These electrochemical devices show high theoretical gravimetric capacity (1672 mAh g^{-1}) and specific energy density (expected value ca. 600Wh kg^{-1}) [43,44]. Electrochemical reactions in the Li-S batteries are multi-step reactions involving different equilibrium states, namely: i) the conversion of S into long-chain Li polysulfides in the high voltage plateau (2.4 V), ii) the reduction of long-chain polysulfides into short-chain polysulfides in the transition state (2.3–2.1 V range) from high to low voltage plateau, and iii) the lithium sulfide (Li_2S) precipitation out from the electrolyte solution in the low voltage plateau (2.1 V) [45]. Since the main limitation of these devices relies on possible undesired phenomena occurring during the battery life cycle (self-discharging, polysulfide shuttle and uncontrolled Li consumption [46,47]), the literature pointed out several strategies to overcome these issues. The most commonly adopted strategy is to confine S into host structures to limit the diffusion of Li polysulfides outside the cathode [48]. In this context, carbonaceous materials are widely exploited to this purpose, and the presence of doping heteroatoms further improves the battery life cycle by increasing both their capacity stability and Coulombic efficiency [49,50]. For these reasons, suitable hosting carbonaceous structures are continuously under consideration by experts in the field.

Therefore, this study aims at investigating the possible exploitation of chitosan-derived biochars as sustainable alternative hosting structures in new generation Li-S batteries. To do this, N-doped biochars were obtained by performing pyrolysis treatments (which are processes easily scalable at the industry level) directly on chitosan powders by choosing "particularly mild" experimental conditions (pyrolysis temperatures were set in the 284–540 °C range).

2. Materials and methods

2.1. Materials

Commercially-available partially N-deacetylated chitosan powder isolated from crab shells (DD = 75–85%, Mv = 190–310 kDa, CAS 9012-76-4, Aldrich) was selected as precursor. Other reagents used were: sodium hydroxide solution (NaOH, purity ≥98.0%, CAS 1310-73-2, Sigma-Aldrich), hydrochloric acid solution (HCl, conc. 37 wt%, CAS 7647-01-0, Fluka), potassium chloride (KCl, purity ≥99.0%, CAS 7447-40-7, Fluka), potassium bromide (KBr, FTIR grade, purity ≥99%, CAS 7758-02-3, Fluka), sulfur (S, CAS 7704-34-9, Sigma-Aldrich), N-methyl-2-pyrrolidone (NMP, CAS 872-50-4, Sigma-Aldrich), polyvinylidene fluoride (PVdF, average Mw 534000, CAS 24937-79-9, Sigma-Aldrich), N-doped high surface area carbon (NC_15, BET surface area 880 m^2 g^{-1}, as in [51]), multi-walled carbon nanotubes (MWCNT, purity ≥98.0%, CAS 308068-56-6, Sigma-Aldrich), and LiTFSI in

TEGME:Diox (conc. 1 M, purity 99.9%, E057, Solvionic). All reagents were used without any further purification.

2.2. Biochar preparation

Pyrolysis treatments were performed following a consolidated procedure from the literature [9,16,39,40], by using a quartz tube reactor LTF 12/38/500 Lenton (tube i.d.: 38mm, heated length: 500mm, quartz cell i.d.: 25 mm, quartz cell length: 750 mm) under inert atmosphere (N_2 flux: 250 mL min^{-1}). Chitosan samples (ca. 2 g) were processed with the following thermal program: heating ramp at 10 °C min^{-1} from room temperature (RT) up to the selected pyrolysis temperature (i.e., either 284 °C, 440 °C or 540 °C), and isothermal step at the pyrolysis temperature for 1 h. Resulting chars were manually crumbled in an agate mortar prior to perform characterization and testing. Samples were labeled with the following acronyms: C284, C440 and C540, according to the pyrolysis temperature, whereas chitosan precursor was labeled as C.

2.3. Physicochemical characterization

Thermo-gravimetric analysis (TGA) on chitosan precursor was performed by means of a TGA Q600 (TA Instruments) under nitrogen flow (flow rate: 100 mL min^{-1}). Measurements (two replicas) were performed by weighting ca. 10 mg of chitosan powder in an open pan of alumina and following the thermal program: heating from RT to 800 °C (heating ramp: 10 °C min^{-1}).

Elemental analysis (in terms of %C, %H, %N, and C/N ratio) of both chitosan and its biochars was determined by means of a Thermo FlashEA 1112 CHNS–O analyzer. Measurements (average values of two replicas) were performed avoiding the presence of water for the calculation, and values presented (expressed as wt% mean value).

Fourier transform infrared (FTIR) spectra of chitosan and its biochars were registered in transmission mode by means of a Bruker Vector 22 spectrophotometer (equipped with Globar source and DTGS detector) working with 128 scans in the 4000–400 cm^{-1} range (resolution: 4 cm^{-1}). Meaurements (three replicas) were performed on KBr pellets (samples:KBr wt. ratio: 1:20).

X-ray diffraction (XRD) patterns were obtained directly on powders by means of PW3040/60 X'Pert PRO MPD diffractometer (PANalytical) with Cu anode, working with Bragg-Brentano geometry (flat sample-holder) at 45 kV and 40 mA. The pattern analysis has been realised by means of the X'Pert High Score instrument database XRD-PDF2-2004.

Scanning electron microscopy (SEM) micrographs of materials' surfaces were registered after sputtering powders with a conductive Au layer (thickness: ca. 15 nm) to avoid charging effects by means of a Bal-tec SCD050 sputter-coater. SEM analysis was performed by means of a ZEISS EVO 50 XVP microscope (equipped with LaB_6 source, secondary electrons collection detector, and EDS probe detector). Measurements were performed by randomly analyzing the samples surface at different magnifications, and the most representative micrographs collected.

Gas-volumetric Kr adsorption experiments at 77 K were performed by means of an ASAP2020 instrument (Micromeritics) to determine the specific surface area (BET model) of biochars [52]. Powders (ca. 0.5–1.0 g) were previously outgassed at 150 °C for 24 h (residual pressure: 10^{-2} mbar) to remove contaminants derived from surface-atmosphere interaction.

Surface charge values of biochars were determined measuring the ζ potential (applying the Smoluchowski equation) [53] by means of electrophoretic light scattering (ELS) (Zetasizer Nano–ZS), with equilibration time 120 s, and 5 replicas per specimen. Measurements (average values of two replicas) were performed by dispersing a fixed amount of each biochar (ca. 10 mg) in a saline solution containing KCl (concentration: 0.01 M, volume: 5 mL) for 1 day and maintaining constant pH (circumneutral, ca. 6) and temperature (ca. 25 °C, indicated in the following as RT). Acid (HCl) and alkaline (NaOH) aqueous solutions were added drop-wise to suspensions for pH correction. Average values were presented (expressed as mean value ± standard deviation, SD in the following) [54].

2.4. Electrochemical characterization

Chitosan-derived biochars were ball milled for 30 min at 300 rpm with 60 wt% of sulfur. Subsequently, the S/biochar mixtures were pretreated with the following thermal program:

a) Heating step from RT to 155 °C (ramp: 0.2 °C min^{-1}).

b) Isothermal step at 155 °C for 5 h.

c) Cooling step from 155 °C to RT (ramp: 0.5 °C min^{-1}).

Electrodes were prepared by mixing the S/biochars mixture with polyvinylidene fluoride (PVdF, as binder) and conductive multiwalled carbon nanotubes (MWCNT, as additive) in an 80:10:10 wt. ratio. The slurry was prepared in N-methyl-2-pyrrolidone (NMP) and casted on a carbon coated Al foil (S loading on carbon-coated Al foil: ca. 1.5 mg cm^{-2}). The two electrode cells were prepared in a pouch type cell inside an Ar filled glovebox. The sulfur cathode (2 cm^2 electrode) was separated from the metallic Li (FMC, 500 μm) anode with Celgard 2400 separator. The electrolyte (1MLiTFSI in TEGDME:Diox (vol% 1:1)) quantity was normalized to 20 μL mgS^{-1}. The batteries were cycled by using Biologic VMP3 galvanostat/potentiostat at a current density of C/10 (167.2 mA g^{-1}) in the 1.5–3.0 V potential range [16].

3. Results and discussion

In order to evaluate the behaviors of the chitosan precursor during the pyrolysis treatment, TGA analysis under nitrogen (inert) atmosphere was performed. Basing on the TG profile reported in Fig. 1, the thermogram of chitosan shows two main weight losses mainly due to: i) the release of physisorbed water molecules (at ca. 100 °C), and ii) the polysaccharide skeletal degradation (principally evolving in the 280–400 °C range but continuing up to 800 °C), thus leaving a carbonaceous residue at 800 °C of ca. 23.18 ± 0.50 wt%. The derivative curve profile evidences both the chitosan's degradation onset temperature (i.e., the temperature at which the degradation phenomena starts) experimentally measured at 284 °C and the maximum rate of decomposition at ca. 300 °C. According to the literature (see [55] and references therein), the thermal degradation of chitosan under inert atmosphere results in a very complex pattern, characterized by formation of a multitude of evolved volatile species, such as H_2O, CO, CO_2, CH_3COOH, CH_4 (the last one released at temperatures higher than 450 °C), NH_3, and pyrazines (mostly including partially-substituted pyridines, pyrroles, and furans). Therefore, based on these results and in analogy to our previous studies [9,16], three different pyrolysis conditions were explored for the chitosan-to-biochar conversion, namely: the experimentally measured onset temperature (284 °C), and two

temperatures set after the chitosan's main degradation phenomenon (respectively at 440 °C and 540 °C, i.e., before and after the release of CH_4 as detected in [55]).

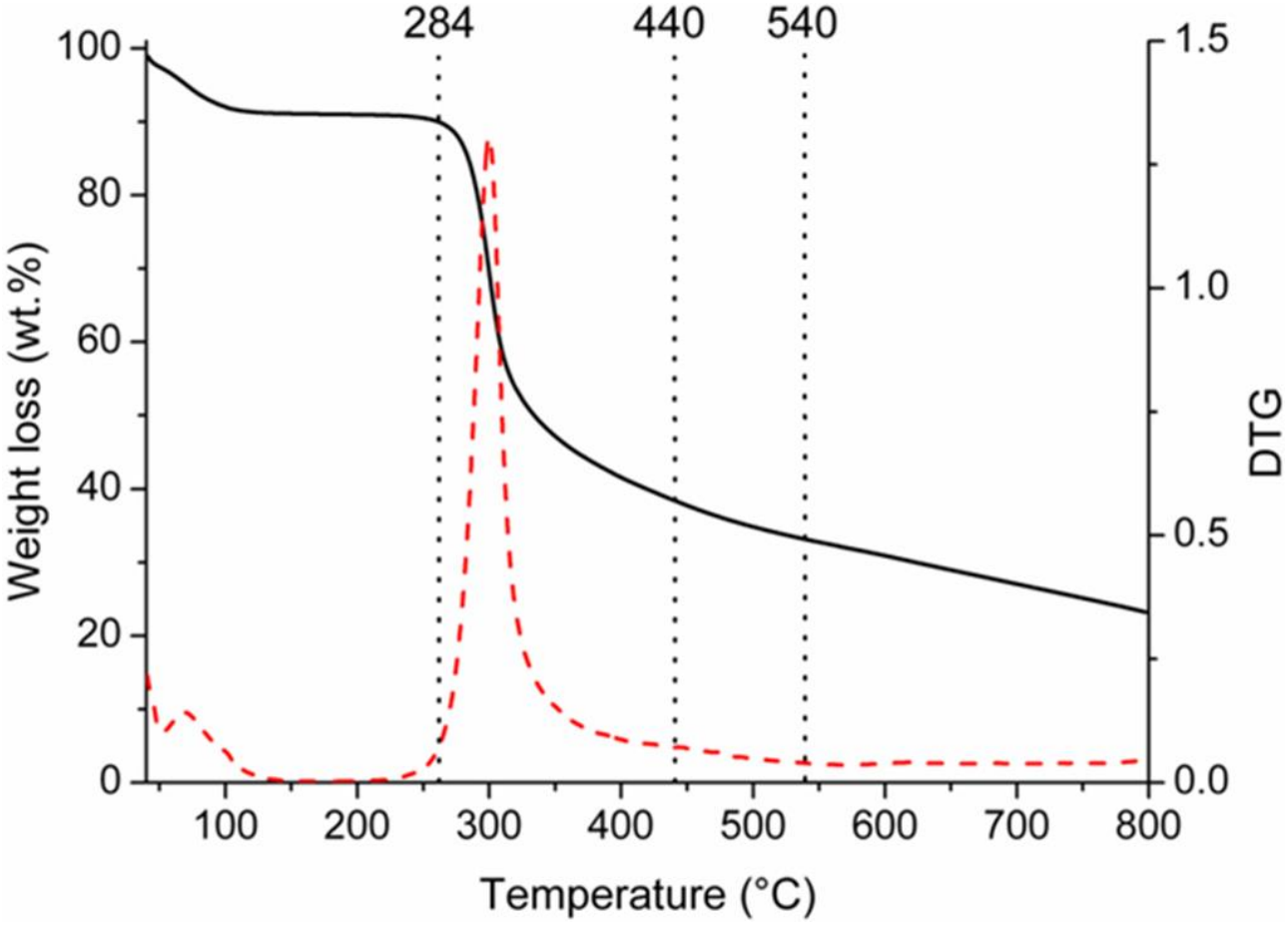

Fig. 1. TG (black solid) and derivative (red dashed) curves of chitosan thermally-treated under nitrogen atmosphere. The black dotted lines refer to the three temperatures investigated for the pyrolysis treatments (namely, the onset 284 °C, 440°Cand 540 °C).

Table 1 reports the elemental composition of chitosan and its chars obtained at the three selected pyrolysis temperatures. The analysis revealed that the thermal treatments caused a general increment of C and N content, and a reduction of H, sign of an overall carbonization of the carbohydrate structure of bare chitosan. Depending on the pyrolysis conditions, the higher the temperature of biochars, the higher the content in C (from 63.3 wt% for C284 to 73.4 wt% for C540), and the lower the H (from ca. 4.7 wt% for C284 to 2.5 wt% for C540). On the contrary, the N content in the chars remained almost constant in the 9.5–10.7 wt% range, thus confirming the formation of N-doped biochars at all pyrolysis conditions here investigated.

Table 1. Elemental composition, BET surface area (measured by Kr adsorption at 77 K), and ζ potential values of bare chitosan (C) and its relative biochars (C284, C440, and C540).

Samples	C (wt%)	H (wt%)	N (wt%)	C/N	BET surface area ($m^2\ g^{-1}$)	ζ potential (mV ± SD)
C	40.2	6.3	5.9	6.8	-	-
C284	63.3	4.7	10.2	6.2	0.83	-31.6 ± 1.2
C440	72.9	3.3	10.7	6.8	0.76	-29.5 ± 1.8
C540	73.4	2.5	9.5	7.7	0.84	-19.1 ± 0.9

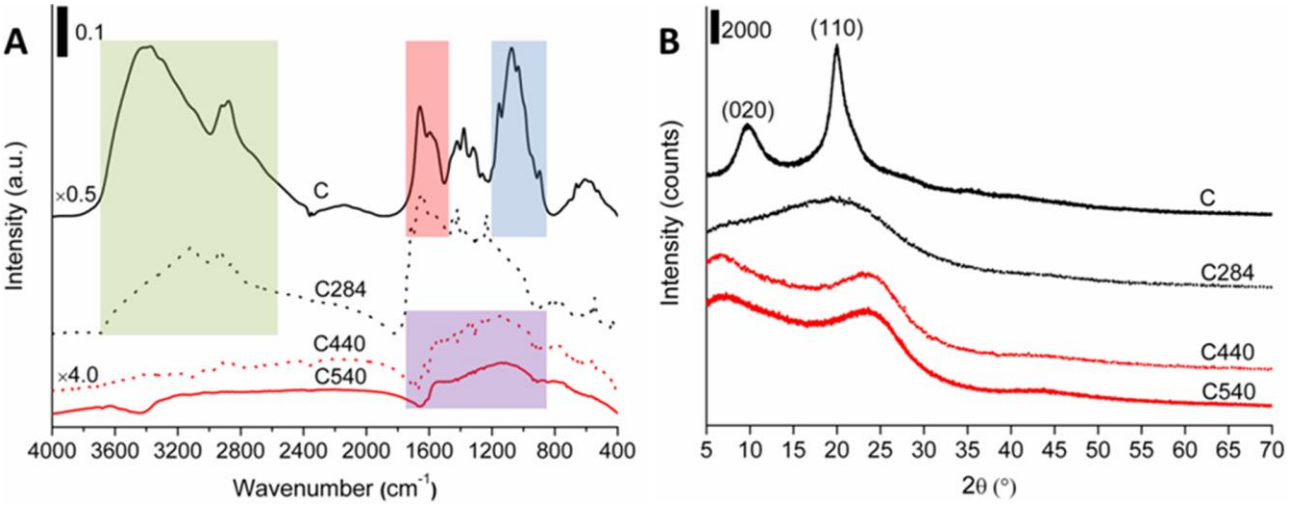

Fig. 2. Absorbance FTIR spectra in the 4000–400 cm−1 range (A) and XRD patterns (B) of chitosan (C, black solid curve), and its biochars C284 (black dotted curve), C440 (red dotted curve), and C540 (red solid curve). The main signals are highlighted and labeled.

In order to better unveil the chemical functionalities present in the biochars, FTIR spectra were registered before (i.e., bare precursor) and after pyrolysis (chitosan-derived biochars) and reported in Fig. 2A. The FTIR spectrum of bare chitosan revealed the main signals, namely: the O-H stretching modes at ca. 3440 cm^{-1}, comprehensive of the spectral components due to N-H vibrations at 3200 cm^{-1}, and the aliphatic C-H stretching modes at ca. 2900 cm^{-1} (Fig. 2A, green box), the characteristic C=O stretching mode of the acetamido moieties (or amide I) at 1660 cm^{-1}, the N-H bending vibration of the amino groups (or amide II) at 1580 cm^{-1} (Fig. 2A, red box), the C-O and C-O-C stretching modes of the glycosidic rings centered at ca. 1000 cm^{-1} (Fig. 2A, blue box) [55,56].

As evidenced by the progressive reduction of the IR signals associated to the hydroxo and amino groups, aliphatic C chains, and glycosidic rings, pyrolysis treatments induced a progressive loss of chemical functionalities, already at the onset condition (i.e., C284). It is interesting to note that the disappearance of OH groups in the hydrated layer of chitosan in sample C284, allows evidencing the presence of N-H stretching bands at about 3200 cm^{-1} of the amino groups present in large amount in chitosan macromolecules. In parallel, increasing the thermal treatment temperature, it is registered the gradual growth of a very broad IR signal in the 1600–1000 cm^{-1} range due to the formation of C-C and C=C bonds of a carbonaceous structure (Fig. 2A, violet box) [32]. In the case of biochars obtained at the higher pyrolysis temperatures, a further reduction of the IR signals was observed.

Biochars surface charge values were determined by performing zeta potential measurements in saline solutions at fixed ionic strength (0.01 M KCl), pH (circumneutral, ca. 6), and temperature (ca. 25 °C, RT). Zeta potential values are reported in Table 1. The analysis revealed that all chitosan-derived biochars show negatively charged surfaces, following the order C540>C440>C284 in absolute values, thus higher the pyrolysis temperature, more negative the zeta potential values, as a consequence of the progressive lack of chitosan functional groups during pyrolysis process.

The XRD analysis in Fig. 2B revealed the structural modifications associated to the crystalline organization of chitosan before and after pyrolysis. As highlighted by the figure, bare chitosan possesses two crystalline reflections, respectively at ca. 2θ=9.7° for the (020) planes and at ca. 19.9° for the (110) planes, as documented in the literature [57]. In accordance to the previously discussed data concerning elemental analysis and FTIR spectroscopy, pyrolysis treatments causes a drastic change in the material structure, with disappearance of the chitosan main signals and formation of a broad amorphous signal at 2θ = 20° at the onset temperature (see the C284 XRD pattern). This should be related to the initial transformation of chitosan which starts losing functional groups, and consequently the large range order towards a more disordered conformation. At higher pyrolysis conditions (namely, 440 °C and 540 °C, i.e., after the main degradation step documented by the TGA profile in Fig. 1), the formation of a new signal at ca. 2θ=25° is observed: this is assignable to the formation of small crystalline domains associated to the organization of (002) graphitic basal plans within the biochars structure [58].

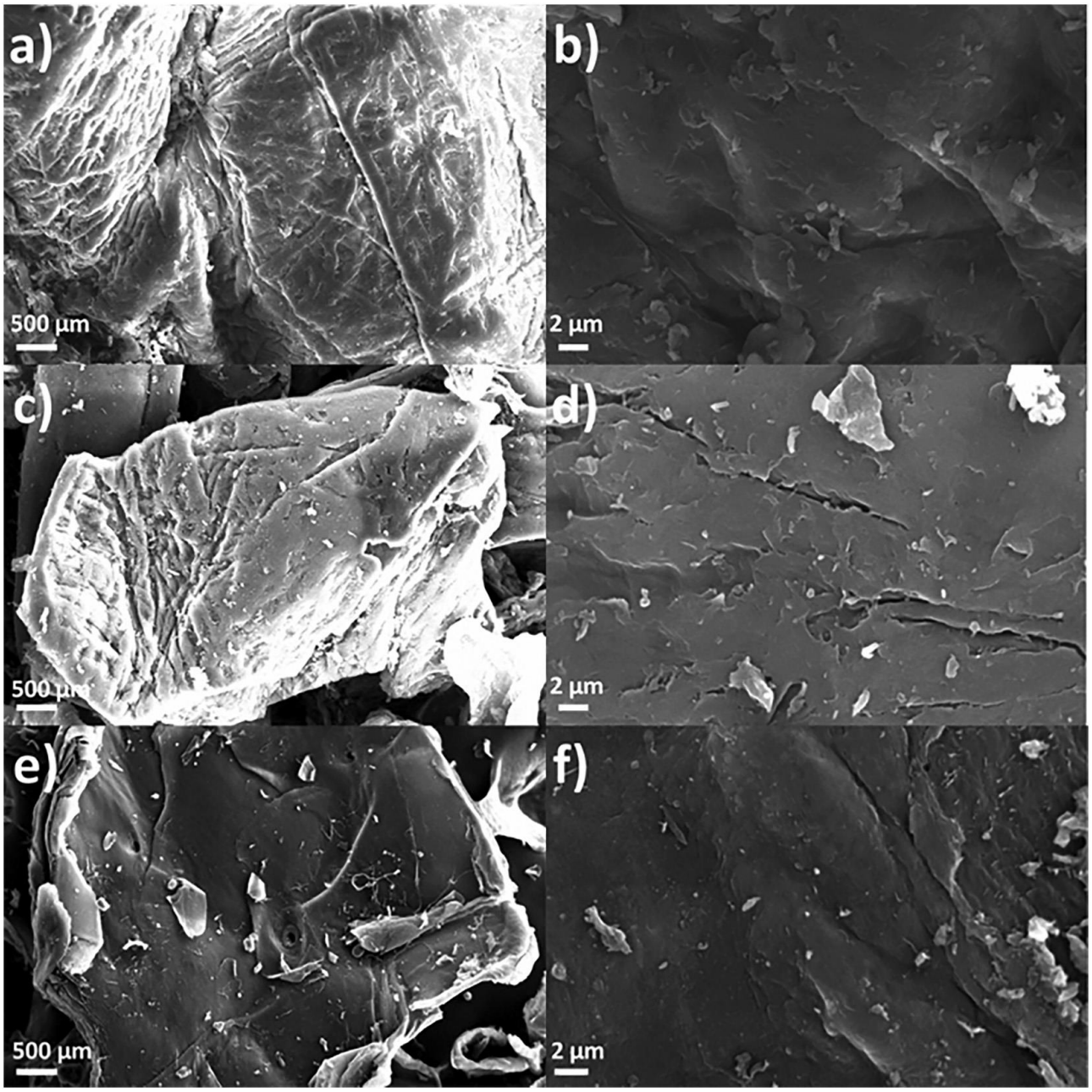

Fig. 3. SEM micrographs at low (left) and high (right) magnification of chitosan-derived biochars C284 (a, b), C440 (c, d), and C540 (e, f).

The morphological analysis of chitosan-derived biochars reported in Fig. 3 revealed in all cases surfaces showing a certain level of roughness, with presence of defects and cracks. Micrographs of C440 and C540 biochars collected at high magnification also demonstrate the formation of some sub-micrometric particles dispersed on the materials' surface. Furthermore, the BET analysis (whose data are summarized in Table 1) revealed in all cases very low values of surface area (ca. 0.76–0.84 m2 g^{-1}), measured by means of Kr adsorption tests at 77 K.

Chitosan-derived N-doped biochars (C284, C440, and C540) were electrochemically tested as sulfur host materials in Li-S batteries. Biochars were impregnated with 60 wt% of sulfur, and samples labeled with the acronym S/biochars (i.e., S/C284, S/C440, and S/C540, respectively). The conductivity of the cathode is achieved through MWCNT wrapping of the S/biochars materials. SEM micrographs of the electrode surface confirmed that the materials are homogeneously distributed

over the cathode surface with absence of cracks and macroscopic defects (data not shown for the sake of brevity). The electrochemical performance of biochars was compared to a reference electrode prepared by using an N-doped high surface area carbon (NC_15, BET surface area 880 m^2 g^{-1}), prepared from glucosamine precursor [51], and impregnated with 60 wt% of sulfur. According to the data reported in Fig. 4, the reference S/NC_15 reached a quite high initial discharge capacity of ca. 1330 mAh gS^{-1}, which dropped down to 1234 mAh gS^{-1} in the 2nd cycle and to 1110 mAh gS^{-1} in the 10th cycle. Concerning the Coulombic efficiency, the reference material S/NC_15 exhibits value below 80% in the initial cycles (a consequence of over-charging due to the polysulfide shuttle phenomena). This undesired phenomenon could be associated to side reactions between electrolyte and high surface area N-doped carbon NC_15, thus resulting in solid-electrolyte interphase (SEI) film formation and consequent electrolyte consumption [59]. Compared to the reference S/NC_15, chitosan-derived N-doped biochars show lower discharge capacity in the initial 40 cycles, but also exhibit lower capacity decay per cycle. After 100 cycles, the retained capacity is higher compared to the S/NC_15. Furthermore, if we compare the three biochars, S/C440 shows the highest first discharge capacity of 874 mAh gS^{-1}, dropping to 828mAh gS^{-1} in the 2nd cycle, and the average Coulombic efficiency during cycling was around 92%.

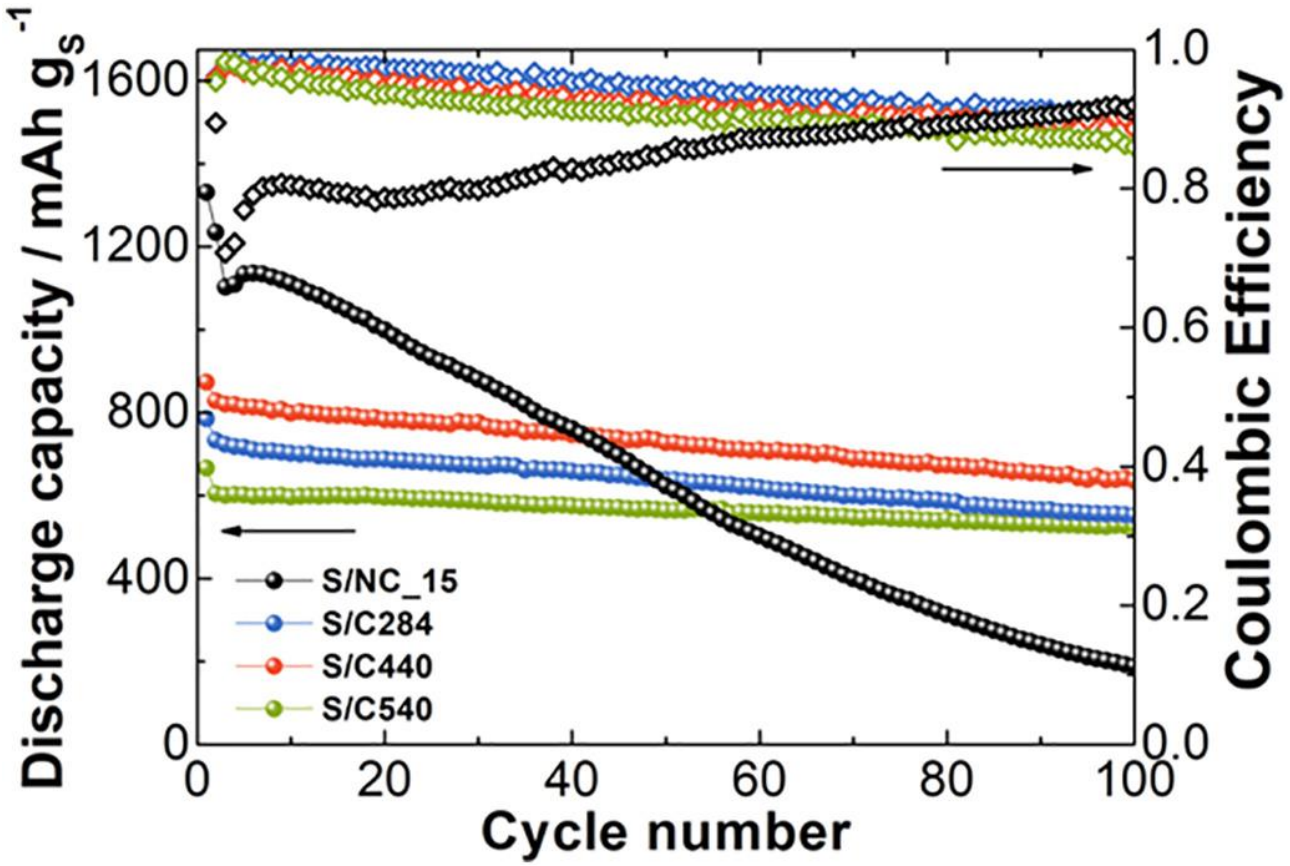

Fig. 4. Discharge capacities (circle symbols, left y axis) and Coulombic efficiency (diamond symbols, right y axis) for the S/biochars: reference material S/NC_15 (black), S/C284 (blue), S/C440 (red) and S/C540 (green).

The S/C284material has cycling behavior similar to S/C440, with approximately 100 mAh gS^{-1} lower discharge capacity, whereas S/C540 exhibits the lowest first discharge capacity of 667 mAh gS^{-1}, dropping to 605 mAh gS^{-1} in the 2nd cycle. Interestingly, S/C540 shows the best capacity retention over cycling (i.e., after 100 cycles, capacity fading only 13%), but the Coulombic efficiency is lower if compared to S/C440 (ca. 90%). The worse performance of the S/C540 compared to the other two

chitosan-derived biochars can be explained by considering the loss of functionalities and heteroatoms doping (nitrogen content) due to higher temperature pyrolysis. However, the three biochars have similar cycling behavior with little differences between each other, with better electrochemical performance (low capacity decay and high Coulombic efficiency) compared to the high surface area N-doped carbon. This result suggests that low surface area carbonaceous substrates prepared at mild conditions might offer an attractive and low-cost alternative for the preparation of energy storage materials.

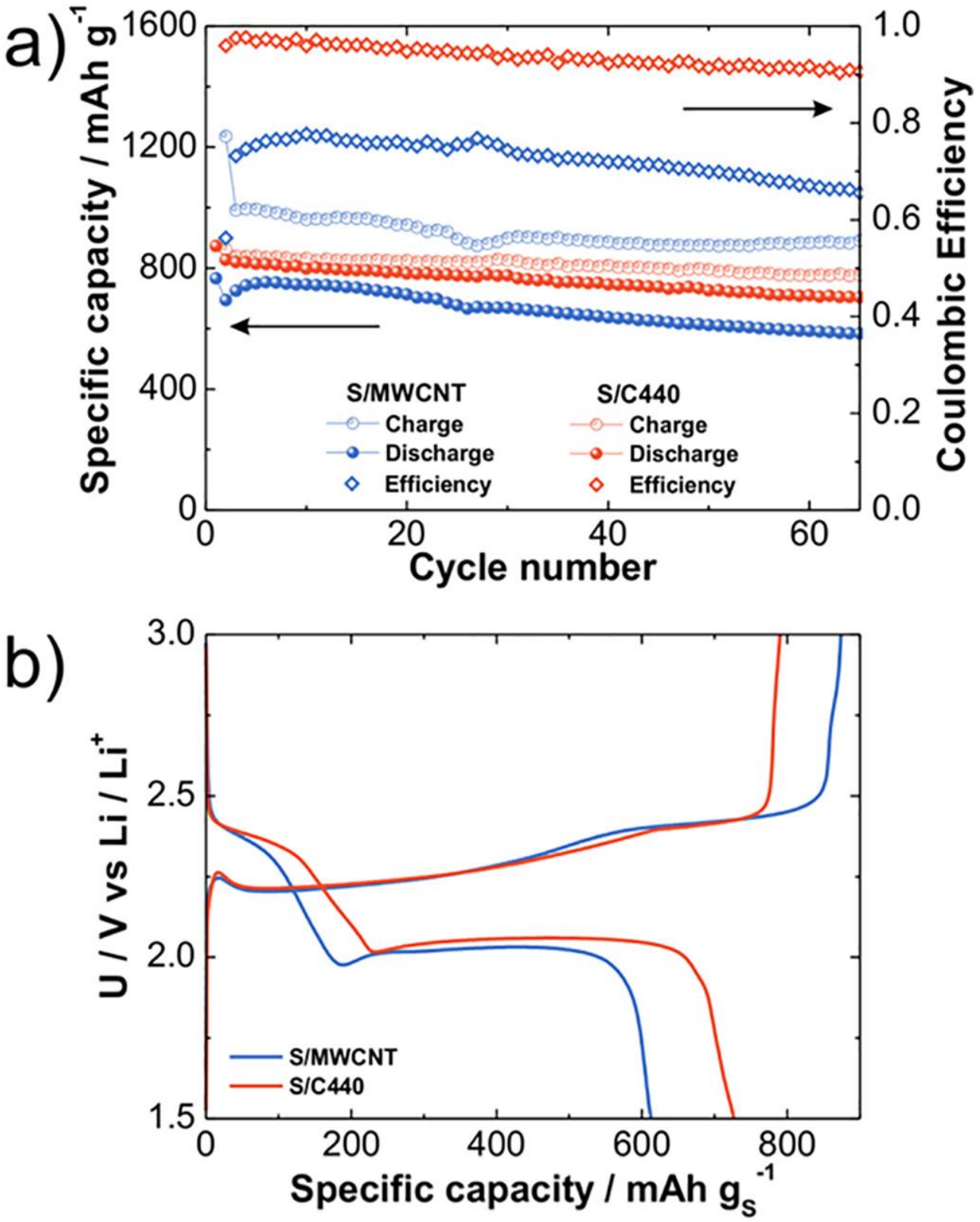

Fig. 5. Panel a) Specific capacity (left y axis) and Coulombic efficiency (right y axis) for S/MWCNT (blue) and S/C440 (red). Panel b) Charge/discharge voltage profiles in the 50th cycle.

The MWCNT additive, which is present inside the cathodes as conductive additive, has a high surface area (280 m2 g^{-1}). In order to test its electrochemical contribution, the electrochemical performance of S/C440 material was further compared against the S/MWCNT material. The cathode with this material was prepared following the same procedure applied to chitosan-derived biochars, namely

by keeping constant the ratio of sulfur to carbon and the sulfur loading on the cathode. Experimental data demonstrate that S/MWCNT delivered an initial specific capacity of 766 mAh gS^{-1} in discharge and 1236 mAh gS^{-1} in charge (Fig. 5a). Such over-charging in Li-S battery system means that the MWCNT material cannot retain and prevent the lithium polysulfides (Li_2S_x) shuttle. The prolonged cycling of this material reveals poor Coulombic efficiency (ca. 70%, a value in good agreement with the presence of Li_2S_x shuttling). Moreover, with the use of C440 carbon an average improvement in discharge capacity of 100 mAh gS^{-1} is observed if compared to the S/MWCNT system. The average Coulombic efficiency during cycling was around 92%, which is significantly better than the Coulombic efficiency of S/MWCNT (as in Fig. 5a). Usually, this trend can be explained by considering the encapsulation of S within the porous carbonaceous cathode [60], but in this case it cannot be a possible explanation as the chitosan-derived biochars host materials did not present a porous system. Such enhanced Coulombic efficiency for the S/C440 system can be explained with a possible better retention of the soluble Li polysulfides by means of the residual polar (O- and N-containing) functional groups of the C440 [61]. Moreover, the capacity fade observed for both S/MWCNT and S/C440 systems is similar. Lastly, Fig. 5b shows that the ratio between the capacities of the high and low voltage plateaus are 30:70 in both materials (i.e., S/MWCNT and S/C440). This behavior suggests that such capacity difference is due to equal loss of all active species in the S/MWCNT, a capacity fade mechanism stemming from Li polysulfides shuttling and loss of cathode active mass material, thus proving the best behaviors of the prepared chitosan-derived biochars as host materials in Li-S batteries.

4. Conclusions

Chitosan, a biopolymer derived from natural biomasses, was selected as low-cost and sustainable precursor for biochar production via pyrolysis treatments performed at very mild conditions, namely at 284 °C (the onset temperature at which the chemical modification of chitosan starts), 440 °C and 540 °C. The produced biochars possess high N-content in the range of 9.5–10.7 wt%, very low BET surface area, and appear as flake-like particles with irregular surface. These carbonaceous substrates were used as sulfur hosting materials in Li-S batteries. The electrodes produced with chitosan-derived biochars present a good homogeneity, good capacity retention and improved Coulombic efficiency if compared to the more conventional high surface area carbon-based and MWCNTs-based systems. Such improved properties are typically due to the encapsulation of sulfur into the hosting material (inside a porous system). However, this cannot be the case of the system here presented since the chitosan-derived biochars here described show no pores. Therefore, the possible explanation of this improved Coulombic efficiency can be associated to a better retention of Li polysulfides due to the presence of residual functionalities in the biochars. This mechanism is an interesting alternative solution respect to the production of porous carbonaceous materials. The good electrochemical performance, associated with low capacity decay and high Coulombic efficiency, pointed out that low surface area carbonaceous substrates prepared at very mild conditions might offer an attractive and low-cost alternative in the preparation of energy storage materials.

Author statement

Roberto Nisticò: Conceptualization, Methodology, Investigation, Data Curation,Writing – Original Draft,Writing – Review & Editing, Visualization, Supervision.

Federico Guerretta: Formal Analysis, Investigation, Data Curation, Writing – Review & Editing, Visualization.

Paola Benzi: Formal Analysis, Investigation, Resources, Data Curation, Writing – Review & Editing.

GiulianaMagnacca: Conceptualization,Methodology, Investigation, Resources, Data Curation, Writing – Review & Editing, Supervision.

Declaration of competing interest

Authors declare that they have no known competing financial interests or personal relationships that could have appeared to influence the work reported in this paper.

Acknowledgements

Authors would like to personally thank Dr. Alen Vizintin (National Institute of Chemistry, Slovenia) for the electrochemical characterization and discussion. Authors would like to thank Prof. Domenica Scarano and Dr. Federico Cesano (University of Torino, Italy), Dr. Maria C. Valsania (University of Torino, Italy) for practical support during SEM analysis, and Dr. Riccardo Leinardi (University of Torino, Italy) for practical support during zeta potential measurements.

Data availability statement

Data will be made available on request.

References

[1] R. Kajaste, Chemicals from biomass – managing greenhouse gas emissions in biorefinery production chains – a review, J. Clean. Prod. 75 (2014) 1–10, https://doi.org/10.1016/j.jclepro.2014.03.070.

[2] A.T. Ubando, C.B. Felix,W.-H. Chen, Biorefineries in circular bioeconomy: a comprehensive review, Bioresour. Technol. 299 (2020), 122585https://doi.org/10.1016/j.biortech.2019.122585.

[3] A. Gandini, T.M. Lacerda, From monomers to polymers from renewable resources: recent advances, Prog. Polym. Sci. 48 (2015) 1–39, https://doi.org/10.1016/j.progpolymsci.2014.11.002.

[4] Z. Wang, M.S. Ganewatta, C. Tang, Sustainable polymers from biomass: bridging chemistry with materials and processing, Prog. Polym. Sci. 101 (2020), 101197https://doi.org/10.1016/j.progpolymsci.2019.101197.

[5] S. Tabasso, M. Ginepro, L. Tomasso, E. Montoneri, R. Nisticò, M. Francavilla, Integrated biochemical and chemical processing of municipal bio-waste to obtain bio based products for multiple uses. The case of soil remediation, J. Clean. Prod. 245 (2020), 119191https://doi.org/10.1016/j.jclepro.2019.119191.

[6] H. Lyu, Q. Zhang, B. Shen, Application of biochar and its composites in catalysis, Chemosphere 240 (2020), 124842https://doi.org/10.1016/j.chemosphere.2019.124842.

[7] J. Placido, S. Bustamante Lopez, K.E.Meissner, D.E. Kelly, S.L. Kelly, Multivariate analysis of biochar-derived carbonaceous nanomaterials for detection of heavy metal ions in aqueous systems, Sci. Total Environ. 688 (2019) 751–761, https://doi.org/10.1016/j.scitotenv.2019.06.342.

[8] J. Wang, S. Wang, Preparation, modification and environmental application of biochar: a review, J. Clean. Prod. 227 (2019) 1002–1022, https://doi.org/10.1016/j.jclepro.2019.04.282.

[9] A. Anceschi, F. Guerretta, G. Magnacca, M. Zanetti, P. Benzi, F. Trotta, F. Caldera, R. Nisticò, Sustainable N-containing biochars obtained at low temperatures as sorbing materials for environmental application: municipal biowaste-derived substances and nanosponges case studies, J. Anal. Appl. Pyrolysis 134 (2018) 606–613, https://doi.org/10.1016/j.jaap.2018.08.010.

[10] W. Zhang, X. Zhang, J. Chen, W. Zou, F. He, X. Hu, D.C.W. Tsang, Y.S. Ok, B. Gao, Biochar technology in wastewater treatment: a critical review, Chemosphere 252 (2020) 126539, https://doi.org/10.1016/j.chemosphere.2020.126539.

[11] X.-F. Sima, Y.-Y. Wang, X.-C. Shen. X.-R. Jing, L.-J. Tian, H.-Q. Yu, H. Jiang, Robust biochar-assisted alleviation of membrane fouling in MBRs by indirect mechanism, Sep. Purif. Technol. 184 (2017) 195–204, https://doi.org/10.1016/j.seppur.2017.04.046.

[12] S. Ding, Y. Liu, Adsorption of CO_2 from flue gas by novel seaweed-based KOH activated porous biochars, Fuel 260 (2020), 116382https://doi.org/10.1016/j.fuel.2019.116382.

[13] P. Pariyar, K. Kumari, M. Kumar Jain, P.S. Jadhao, Evaluation of change in biochar properties derived from different feedstock and pyrolysis temperature for environmental and agricultural application, Sci. Total Environ. 713 (2020) 136433, https://doi.org/10.1016/j.scitotenv.2019.136433.

[14] C. del Mar Saavedra Rios, V. Simone, L. Simonin, S. Martinet, C. Dupont, Biochars from various biomass types as precursors for hard carbon anodes in sodium-ion batteries, Biomass Bioenergy 117 (2018) 32–37, https://doi.org/10.1016/j.biombioe.2018.07.001.

[15] B.-H. Cheng, R.J. Zeng, H. Jiang, Recent developments of post-modification of biochar for electrochemical energy storage, Bioresour. Technol. 246 (2017) 224–233, https://doi.org/10.1016/j.biortech.2017.07.060.

[16] G. Magnacca, F. Guerretta, A. Vizintin, P. Benzi, M.C. Valsania, R. Nisticò, Preparation, characterization and environmental/electrochemical energy storage testing of low cost biochar from natural chitin obtained via pyrolysis at mild conditions, Appl. Surf. Sci. 427 (2018) 883–893, https://doi.org/10.1016/j.apsusc.2017.07.277.

[17] Q. Zhang, D. Zhang, H. Xu, W. Xu, W. Lu, X. Ren, H. Cai, H. Lei, E. Huo, Y. Zhao, M. Qian, X. Lin, E.M. Villota, W. Mateo, Biochar filled high-density polyethylene composites with excellent properties: towards maximizing the utilization of agricultural wastes, Ind. Crop. Prod. 146 (2020) 112185, https://doi.org/10.1016/j.indcrop.2020.112185.

[18] X.Wang, F. Sotoudehniakarani, Z. Yu, J.J. Morrell, J. Cappellazzi, A.G. McDonald, Evaluation of corrugated cardboard biochar as reinforcing fiber on properties, biodegradability and weatherability of wood-plastic composites, Polym. Degrad. Stab. 168 (2019), 108955https://doi.org/10.1016/j.polymdegradstab. 2019.108955.

[19] S. Gupta, H.W. Kua, C.Y. Low, Use of biochar as carbon sequestering additive in cement mortar, Cem. Concr. Compos. 87 (2018) 110–129, https://doi.org/10.1016/j.cemconcomp.2017.12.009.

[20] R. Nisticò, L. Lavagna, D. Versaci, P. Ivanchenko, P. Benzi, Chitosan and its char as fillers in cement-base composites: a case study, Boletín de la Sociedad Española de Cerámica y Vidrio (2020) https://doi.org/10.1016/j.bsecv.2019.10.002 (in press).

[21] F.M. Kerton, Y. Liu, K.W. Omari, K. Hawboldt, Green chemistry and the ocean-based biorefinery, Green Chem. 15 (2013) 860–871, https://doi.org/10.1039/C3GC36994C.

[22] R. Nisticò, Aquatic-derived biomaterials for a sustainable future: a European opportunity, Resources 6 (2017) 65, https://doi.org/10.3390/resources6040065.

[23] S.M. Ahsan, M. Thomas, K.K. Reddy, S.G. Sooraparaju, A. Asthana, I. Bhatnagar, Chitosan as biomaterial in drug delivery and tissue engineering, Int. J. Biol. Macromol. 110 (2018) 97–109, https://doi.org/10.1016/j.ijbiomac.2017.08.140.

[24] Z. Shariatinia, Pharmaceutical applications of chitosan, Adv. Colloid Interf. Sci. 263 (2019) 131–194, https://doi.org/10.1016/j.cis.2018.11.008.

[25] P. Avetta, R. Nisticò, M.G. Faga, D. D'Angelo, E. Aimo Boot, R. Lamberti, S. Martorana, P. Calza, D. Fabbri, G. Magnacca, Hernia-repair prosthetic devices functionalised with chitosan and ciprofloxacin coating: controlled release and antibacterial activity, J. Mater. Chem. B 2 (2014) 5287–5294, https://doi.org/10.1039/c4tb00236a.

[26] C.R. Afonso, R.S. Hirano, A.L. Gaspar, E.G.L. Chagas, R.A. Carvalho, F.V. Silva, G.R. Leonardi, P.S. Lopes, C.F. Silva, C.M.P. Yoshida, Biodegradable antioxidant chitosan films useful as an anti-aging skin mask, Int. J. Biol. Macromol. 132 (2019) 1262–1273, https://doi.org/10.1016/j.ijbiomac.2019.04.052.

[27] S. Sarode, P. Upadhyay, M.A. Khosa, T. Mak, A. Shakir, S. Song, A. Ullah, Overview of wastewater treatment methods with special focus on biopolymer chitin-chitosan, Int. J. Biol. Macromol. 121 (2019) 1086–1100, https://doi.org/10.1016/j.ijbiomac.2018.10.089.

[28] R. Nisticò, F. Franzoso, F. Cesano, D. Scarano, G. Magnacca, M.E. Parolo, L. Carlos, Chitosan-derived iron oxide systems for magnetically guided and efficient water purification processes from polycyclic aromatic hydrocarbons, ACS Sustain. Chem. Eng. 5 (2017) 793–801, https://doi.org/10.1021/acssuschemeng.6b02126.

[29] M.E. Peralta, R. Nisticò, F. Franzoso, G.Magnacca, L. Fernandez, M.E. Parolo, E. Garcia Leon, L. Carlos, Highly efficient removal of heavy metals from waters by magnetic chitosan-based composite, Adsorption 25 (2019) 1337–1347, https://doi.org/10.1007/s10450-019-00096-4.

[30] R. Priyadarshi, J.-W. Rhim, Chitosan-based biodegradable functional films for food packaging applications, Innovative Food Sci. Emerg. Technol. 62 (2020), 102346, https://doi.org/10.1016/j.ifset.2020.102346.

[31] P.L. Kashyap, X. Xiang, P. Heiden, Chitosan nanoparticle based delivery systems for sustainable agriculture, Int. J. Biol. Macromol. 77 (2015) 36–51, https://doi.org/10.1016/j.ijbiomac.2015.02.039.

[32] H. Kaczmarek, J. Zawadzki, Chitosan pyrolysis and adsorption properties of chitosan and its carbonizate, Carbohydr. Res. 345 (2010) 941–947, https://doi.org/10.1016/j.carres.2010.02.024.

[33] IBI, Standardized product definition and product testing guidelines for biochar that is used in soil – version 2.1, international biochar initiative, (November 2015). IBISTD-2.1. Available on-line at http://www.biochar-international.org/characterizationstandard 2015. (Accessed 5 May 2020).

[34] Y. Qiao, F. Kong, C. Zhang, R. Li, A. Kong, Y. Shan, Highly efficient oxygen electrode catalyst derived from chitosan biomass by molten salt pyrolysis for zinc-air battery, Electrochim. Acta 339 (2020), 135923https://doi.org/10.1016/j.electacta.2020135923.

[35] M.A.O. Lourenco, C. Nunes, J.R.B. Gomes, J. Pires, M.L. Pinto, P. Ferreira, Pyrolyzed chitosan-based materials for CO_2/CH_4 separation, Chem. Eng. J. 362 (2019) 364–374, https://doi.org/10.1016/j.cej.2018.12.180.

[36] X. Chen, W.-D. Oh, P.-H. Zhang, R.D. Webster, T.-T. Lim, Surface construction of nitrogen-doped chitosan-derived carbon nanosheets with hierarchically porous structure for enhanced sulfacetamide degradation via peroxymonosulfate activation: maneuverable porosity and active sites, Chem. Eng. J. 382 (2020), 122908https://doi.org/10.1016/j.cej.2019.122908.

[37] M. Bengisu, E. Yilmaz, Oxidation and pyrolysis of chitosan as a route for carbon fiber derivation, Carbohydr. Polym. 50 (2002) 165–175, https://doi.org/10.1016/S0144-8617(02)00018-8.

[38] R. Yi, W. Cai, C. Dang, B. Han, L. Liu, J. Fan, Mild hydrothermal preparation of millimiter-sized carbon beads from chitosan with significantly improved adsorption stability for Cr(VI), Chem. Eng. Res. Des. 156 (2020) 43–53, https://doi.org/10.1016/j.cherd.2020.01.026.

[39] F. Guerretta, G. Magnacca, F. Franzoso, P. Ivanchenko, R. Nisticò, Sodium alginate conversion into char via pyrolysis at the onset temperature, Mater. Lett. 234 (2019) 339–342, https://doi.org/10.1016/j.matlet.2018.09.127.

[40] R. Nisticò, F. Guerretta, P. Benzi, G. Magnacca, D. Mainero, E. Montoneri, Thermal conversion of municipal biowaste anaerobic digestate to valuable char, Resources 8 (2019) 24, https://doi.org/10.3390/resources8010024.

[41] C. Zhang, Z. Zhang, L. Zhang, Q. Li, C. Li, G. Chen, S. Zhang, Q. Liu, X. Hu, Evolution of the functionalities and structures of biochars in pyrolysis of poplar in a wide temperature range, Bioresour. Technol. 304 (2020), 123002https://doi.org/10.1016/j.biortech.2020.123002.

[42] P.G. Bruce, S.A. Fraunberger, L.J. Hardwick, J.-M. Tarascon, Li-O2 and Li-S batteries with high energy storage, Nat. Mater. 11 (2012) 19–29, https://doi.org/10.1038/nmat3191.

[43] M. Hagen, D. Hanselmann, K. Ahlbrecht, R. Maca, D. Gerber, J. Tubke, Lithium-sulfur cells: the gap between the state-of-the-art and the requirements for high energy battery cells, Adv. Energy Mater. 5 (2015), 1401986https://doi.org/10.1002/aenm.201401986.

[44] A. Roseman, E. Markevich, G. Salitra, D. Aurbach, A. Garsuch, F.F. Chesneau, Review on Li-sulfur battery systems: an integral perspective, Adv. Energy Mater. 5 (2015) 1500212, https://doi.org/10.1002/aenm.201500212.

[45] R. Dominko, M.U.M. Patel, V. Lapornik, A. Vizintin, M. Kozelj, N.N. Tusar, I. Arcon, L. Stievano, G. Aquilanti, Analytical detection of polysulfides in the presence of adsorption additives by operand X-ray adsorption spectroscopy, J. Phys. Chem. C 119 (2015) 19001–19010, https://doi.org/10.1021/acs.jpcc.5b05609.

[46] Y.-X. Yin, S. Xin, Y.-G. Guo, L.J.Wan, Lithium-sulfur batteries: electrochemistry, materials, and prospects, Angew. Chem. Int. Ed. 52 (2013) 13186–13200, https://doi.org/10.1002/anie.201304762.

[47] A. Manthiram, Y. Fu, S.-H. Chung, C. Zu, Y.-S. Su, Rechargeable lithium-sulfur batteries, Chem. Rev. 114 (2014) 11751–11787, https://doi.org/10.1021/cr500062v.

[48] S. Evers, L.F. Nazar, New approaches for high energy density lithium-sulfur battery cathodes, Acc. Chem. Res. 46 (2013) 1135–1143, https://doi.org/10.1021/ar3001348.

[49] X.G. Sun, X. Wang, R.T. Mayes, S. Dai, Lithium-sulfur batteries based on nitrogen doped carbon and an ionic-liquid electrolyte, ChemSusChem 5 (2012) 2079–2085, https://doi.org/10.1002/cssc.201200101.

[50] J.P. Paraknowitsch, Y. Zhang, B.Wienert, A. Thomas, Nitrogen- and phosphorous-codoped carbons with tunable enhanced surface areas promoted by the doping additives, Chem. Commun. 49 (2013) 1208–1210, https://doi.org/10.1039/C2CC37398J.

[51] F. Schipper, A. Vizintin, J. Ren, R. Dominko, T.-P. Fellinger, Biomass-derived heteroatom-doped carbon aerogels from a salt melt sol-gel synthesis and their performance in Li-S batteries, ChemSusChem 8 (2015) 3077–3083, https://doi.org/10.1002/cssc.201500832.

[52] S. Brunauer, P.H. Emmett, E. Teller, Adsorption of gases in multimolecular layers, J. Am. Chem. Soc. 60 (1938) 309–319, https://doi.org/10.1021/ja01269a023.

[53] L. Jiang, L. Gao, J. Sun, Production of aqueous colloidal dispersions of carbon nanotubes, J. Colloid Interface Sci. 260 (2003) 89–94, https://doi.org/10.1016/S0021-9797(02)00176-5.

[54] R. Nisticò, L.R. Celi, A. Bianco Prevot, L. Carlos, G. Magnacca, E. Zanzo, M. Martin, Sustainable magnet-responsive nanomaterials for the removal of arsenic from contaminated water, J. Hazard. Mater. 342 (2018) 260–269, https://doi.org/10.1016/j.jhazmat.2017.08.034.

[55] I. Corazzari, R. Nisticò, F. Turci, M.G. Faga, F. Franzoso, S. Tabasso, G. Magnacca, Advanced physico-chemical characterization of chitosan by means of TGA coupled on-line with FTIR and GCMS: thermal degradation and water adsorption capacity, Polym. Degrad. Stab. 112 (2015) 1–9, https://doi.org/10.1016/j.polymdegradstab.2014.12.006.

[56] M.R. Kasaai, A review of several reported procedures to determine the degree of N-acetylation for chitin and chitosan using infrared spectroscopy, Carbohydr. Polym. 71 (2008) 497–508, https://doi.org/10.1016/j.carbpol.2007.07.009.

[57] J. Kumirska,M. Czerwicka, Z. Kaczyński, A. Bychowska, K. Brzozowski, J. Thöming, P. Stepnowski, Application of spectroscopic methods for structural analysis of chitin and chitosan, Mar. Drugs 8 (2010) 1567–1636, https://doi.org/10.3390/md8051567.

[58] A.K. Kercher, D.C. Nagle, Microstructural evolution during charcoal carbonization by X-ray diffraction analysis, Carbon 41 (2003) 15–27, https://doi.org/10.1016/S0008-6223(02)00261-0.

[59] P. Zheng, T. Liu, S. Guo, Micro-nano structure hard carbon as a high performance anode material for sodium-ion batteries, Sci. Rep. 6 (2016) 35620, https://doi.org/10.1038/srep35620.

[60] D. Gueon, M.-Y. Ju, J.H. Moon, Complete encapsulation of sulfur through interfacial energy control of sulfur solutions for high-performance Li-S batteries, Proc. Natl. Acad. Sci. U.S.A. 117 (2020) 12686–12692, https://doi.org/10.1073/pnas.2000128117.

[61] P. Zhu, J. Song, D. Lv, D.Wang, C. Jaye, D.A. Fischer, T.Wu, Y. Chen, Mechanism of enhanced carbon cathode performance by nitrogen doping in lithium-sulfur battery: an X-ray absorption spectroscopic study, J. Phys. Chem. C 118 (2014) 7765–7771, https://doi.org/10.1021/jp4123634.